Local tissue interactions govern pLL patterning in medaka

Ali Seleit [a,b,1], Karen Gross [a,b], Jasmin Onistschenko [a,b], Oi Pui Hoang [a], Jonas Theelke [a,2], Lázaro Centanin [a,*]

[a] *Laboratory of Clonal Analysis of Post-Embryonic Stem Cells, Centre for Organismal Studies (COS) Heidelberg, Im Neuenheimer Feld 230, Universität Heidelberg, 69120, Heidelberg, Germany*
[b] *Heidelberg Biosciences International Graduate School (HBIGS), Universität Heidelberg, Heidelberg, Germany*

A B S T R A C T

Vertebrate organs are arranged in a stereotypic, species-specific position along the animal body plan. Substantial morphological variation exists between related species, especially so in the vastly diversified teleost clade. It is still unclear how tissues, organs and systems can accommodate such diverse scaffolds. Here, we use the distinctive arrangement of neuromasts in the posterior lateral line (pLL) system of medaka fish to address the tissue-interactions defining a pattern. We show that patterning in this peripheral nervous system is established by autonomous organ precursors independent of neuronal wiring. In addition, we target the *keratin 15* gene to generate *stuck-in-the-midline (siml)* mutants, which display epithelial lesions and a disrupted pLL patterning. By using *siml/wt* chimeras, we determine that the aberrant *siml* pLL pattern depends on the mutant epithelium, since a *wild type* epithelium can rescue the *siml* phenotype. Inducing epithelial lesions by 2-photon laser ablation during pLL morphogenesis phenocopies *siml* genetic mutants and reveals that epithelial integrity defines the final position of the embryonic pLL neuromasts. Our results using the medaka pLL disentangle intrinsic from extrinsic properties during the establishment of a sensory system. We speculate that intrinsic programs guarantee proper organ morphogenesis, while instructive interactions from surrounding tissues facilitates the accommodation of sensory organs to the diverse body plans found among teleosts.

1. Introduction

Among the members of an animal species, organs are arranged in fixed numbers and stereotypic positions along the body. Subtle or major variations that occur between related species have necessarily evolved by maintaining organ functionality and association with the rest of the tissues in the organism. There is a plethora of body sizes and patterns in the animal kingdom, where teleost fish in particular have mastered body alteration and re-shaping. How the different tissues, organs and systems can scale and accommodate to such diverse scaffolds is still poorly understood. So is the impact of changes in one tissue on another, *i.e* the hierarchical organisation governing these changes.

The reproducibility of developmental programs during organogenesis appears to be an intrinsic property of the system. This has been demonstrated by self-organizing systems over the last decade, using different organoid models (Eiraku et al., 2011; Lancaster et al., 2013; Sato et al., 2009; Turner et al., 2016; van den Brink et al., 2014). Organ location, on

the other hand, is achieved in two different manners depending on the animal model. Cases like *C. elegans* constitute a clear example of a fixed, deterministic lineage where the precise temporal and spatial order guarantees the formation of cell types and tissues in a *defined* location (Sulston et al., 1983). Most vertebrates analysed, however, follow a different developmental logic where an initial symmetry break will induce the appearance of different cell types, tissues and eventually organs (Martinez Arias and Steventon, 2018). Induction events constitute examples of how cell types and tissues interact with each other to instruct their timely appearance at *relative* locations. The rationale that emerges for vertebrate organogenesis is that of an initial plasticity - *the place* in which the organs will be formed, largely influenced by the body shape of the organism - followed by a fixed, self-organizing programme - *they way* in which organogenesis will take place. While molecular programs orchestrating organogenesis have been followed in numerous species, the way tissue interactions could result in new patterns during development remains largely unknown.

The lateral line is a sensory system whose organs, the neuromasts, distribute along the surface of fish and aquatic amphibia (Ghysen and Dambly-Chaudière, 2007; Sapède et al., 2002). Their exposed location and unique morphology have made them a popular model to tackle several aspects of organogenesis. Many groups have contributed to our extensive understanding of the signalling pathways shaping the embryonic posterior lateral line system (pLL, from here on) in zebrafish (Aman and Piotrowski, 2008; Chitnis et al., 2012; David et al., 2002; Grant et al., 2005; Haas and Gilmour, 2006; Hernández et al., 2006; Lecaudey et al., 2008; López-Schier and Hudspeth, 2005; Lush and Piotrowski, 2014; Ma et al., 2008; Nechiporuk and Raible, 2008; Pinto-Teixeira et al., 2015; Romero-Carvajal et al., 2015; Sánchez et al., 2016; Wada et al., 2013a; Wibowo et al., 2011). Briefly, a primordium migrates along the horizontal myoseptum and deposits a handful of pre-formed neuromasts from

its rear edge (Ghysen and Dambly-Chaudière, 2007; Grant et al., 2005; Lecaudey et al., 2008; López-Schier and Hudspeth, 2005; Lush and Piotrowski, 2014; Nechiporuk and Raible, 2008). Additional primordia will migrate later, expanding the initial set of organs during the larval stages (Ghysen and Dambly-Chaudière, 2007; Sapède et al., 2002; Ledent, 2002; Nuñez et al., 2009; Whitfield, 2005). Some aspects of lateral line formation have been reported as well in different fish species, including tuna, *Astyanax* and medaka (Sapède et al., 2002; Ghysen et al., 2010, 2012; Pichon and Ghysen, 2004; Seleit et al., 2017a, 2017b). The availability of transgenic lines (*Tg* from here on) and other genetic tools in medaka allowed a dynamic study of neuromast generation, which revealed that one primordium is responsible for the sequential generation of two different, parallel lateral lines (Seleit et al., 2017a). A first set of neuromasts is deposited by the primordium (*primary* neuromasts) and
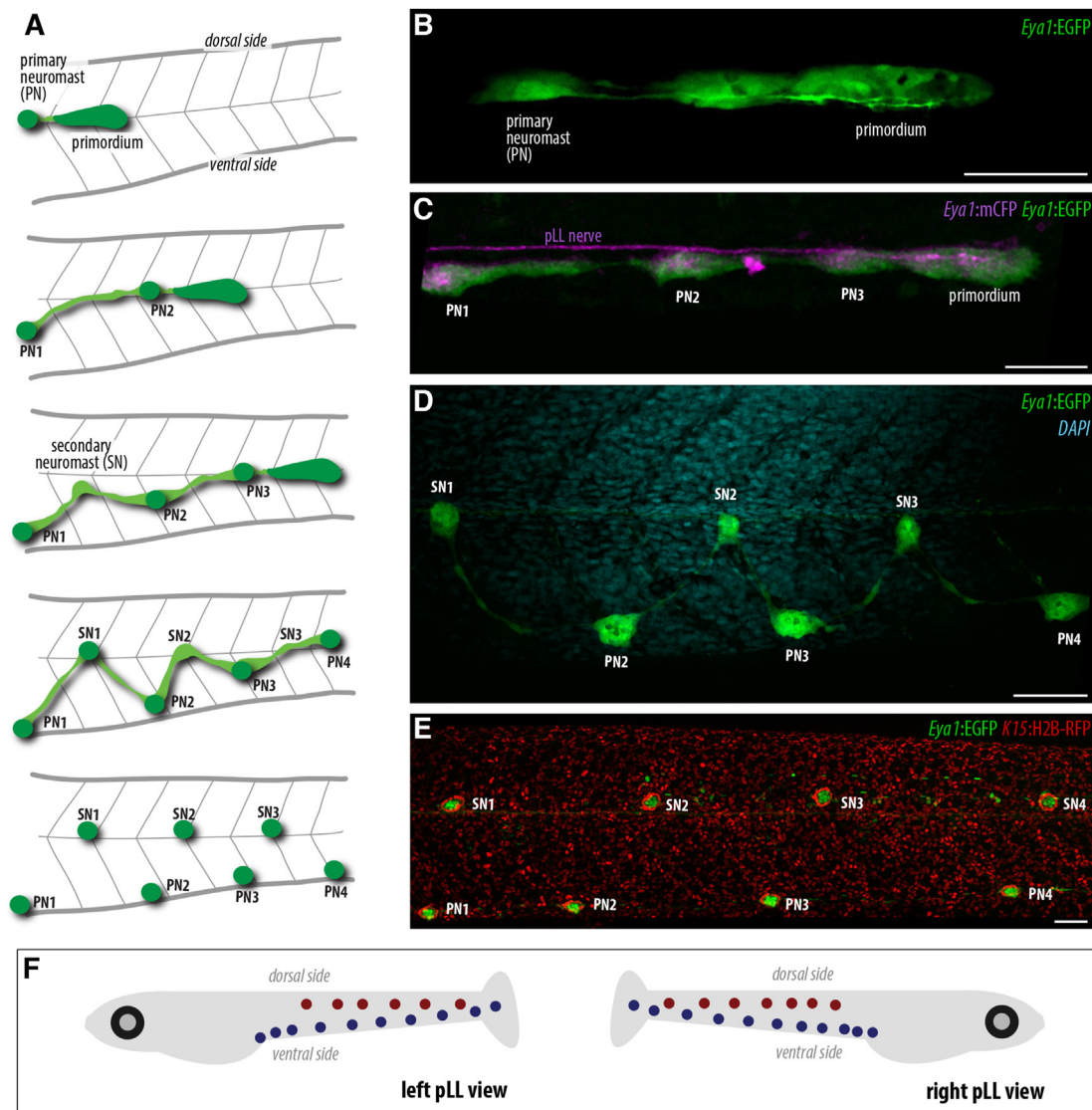

Fig. 1. The formation of the posterior lateral line (pLL) system in medaka.
(**A** top, **B**) A primordium detaches from the pLL placode and migrates posteriorly, depositing neuromasts along the myoseptum. Both the primordium and the deposited neuromasts are labelled in Tg(*Eya1*:EGFP). (**C**) Primary neuromasts (PN) move ventrally immediately after deposition (A, second upper panel). The membrane-tagged fluorescent protein of Tg(*Eya1*:mCFP) accumulates preferentially in the pLL nerve, which travels along the myoseptum following the pLL primordium. Along the manuscript, we use Tg(*Eya1*:EGFP) to label the pLL primordium and the deposited neuromasts, and Tg(*Eya1*:mCFP) to highlight the pLL nerve. (**D**, A third and fourth schemes) Secondary neuromasts (SNs) form between each pair of primary neuromasts, and these SNs migrate dorsally reaching the midline to form a characteristic zig-zag pattern. (**E**, A bottom scheme) By the end of embryogenesis, the pLL is composed of two parallel lines: a ventral pLL formed by primary neuromasts, and a midline pLL formed by secondary neuromasts. Scale bar = 50 μm. Anterior is to the left and dorsal is up in all panels. (**F**) Of note, fish have a left and a right lateral line system, each generated by a different primordium. The process described in A-E occurs at the left side of the trunk and at the right side of the trunk, and involves independent pLL primordia for each. The convention for the rest of the figures is dorsal side up, anterior to the left.

move ventrally immediately after deposition to form the ventral pLL. Later, a second set of organs (*secondary* neuromasts) is formed between each pair of primary neuromasts and migrate dorsally to form the midline pLL (Fig. 1). Besides their final position, primary and secondary organs can be distinguished from each other using two additional criteria. First, primary organs have a clear pLL nerve connection as soon as they are released from the posterior end of the migrating primordium, while secondary organs form their nerve connection after organogenesis. Second, primary organs are much bigger than secondaries during embryonic development, since secondaries are initially formed from an aggregation of just 6–10 inter-neuromast cells — taking a few days for them to reach a size that is equivalent to that of primary neuromasts. Unlike other species, pLL neuromasts in medaka do not occupy every single somite boundary (*vertical* myoseptum) along the tail. Often, the number of neuromasts in the left pLL also differ from that in the right pLL (Seleit

et al., 2017a). The posterior lateral line in medaka at the end of embryogenesis, therefore, represents a unique neuromast pattern that deviates from that of previously studied fish.

Here, we use the sequential formation and opposite migration of neuromasts in medaka to address the tissue interactions necessary to build a pattern. By using 2-photon laser ablations we discard any role for the lateral line nerve and the associated glial cells in pLL patterning. We then analyse medaka mutants with duplicated body sectors and show that primary neuromasts resolve organ positioning in an autonomous manner. Despite autonomous neuromast location, our 4D analysis reveals intrinsic properties of the pLL as a system. Namely, one secondary organ forms in between two primaries, and all secondary neuromasts inevitably locate to the midline. In addition, we generate viable *keratin 15* mutants with novel pLL patterns and by transplantation experiments provide strong evidence that the integrity of the epidermis influences the
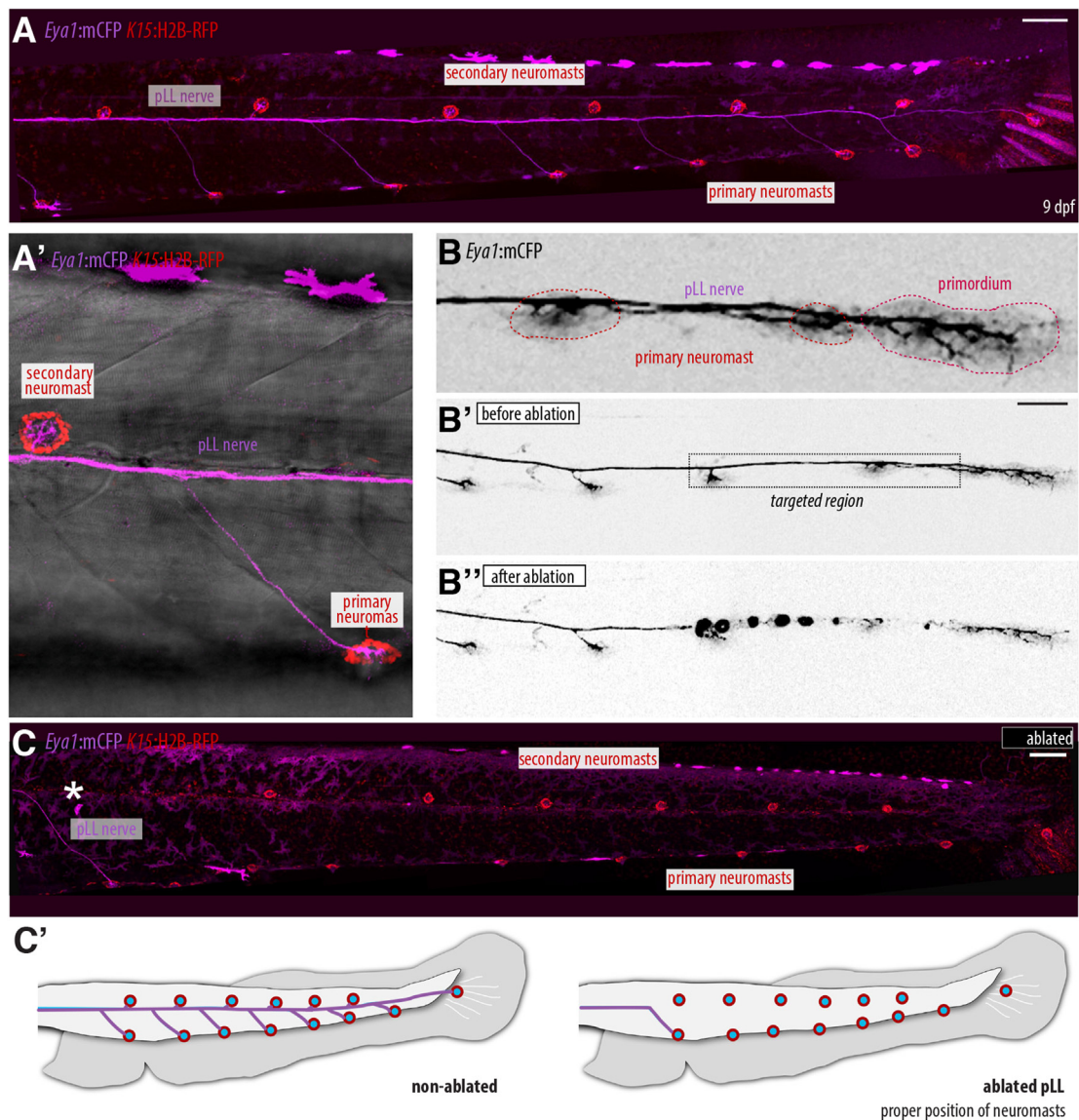

Fig. 2. Correct organ numbers and positions in pLL of medaka despite loss of pLL nerve
(**A-A′**) Control 9 dpf Tg(*Eya1*:mCFP)(*K15*:H2B-RFP) embryo displays alternating neuromasts in the pLL. The pLL nerve is labelled by *Eya1*:mCFP along the trunk and is connected to the mature primary ventral organs and midline secondary organs that are both labelled by *K15*:H2B-RFP. (**B**) 3–4 dpf Tg(*Eya1*:mCFP) medaka embryo highlighting the primordium, the pLL nerve and deposited primary neuromasts along the horizontal myoseptum. (**B′**) 3–4 dpf Tg(*Eya1*:mCFP) medaka embryo before multi-photon laser ablation; primordium is migrating and a few organs have been deposited. (**B″**) 3–4 dpf Tg(*Eya1*:mCFP) medaka embryo after multi-photon ablation; a segment of the pLL nerve is ablated while neuromasts and primordium remain intact and un-injured. (**C**) Pattern and number of neuromasts are normal despite loss of pLL nerve in Tg(*Eya1*:mCFP) (*K15*:H2B-RFP) 9 dpf. (N = 11 embryos). White asterisk indicates ablation site. (**C′**) Scheme of neuromast position and number upon ablation of the pLL. Scale bar = 100 μm.

embryonic pattern of the medaka pLL. We confirm these results by mechanically interfering with epithelial integrity locally and recapitulate the patterning defects observed in our *krt15* mutants. Our results strongly suggest that tissue interactions govern pLL pattern formation and that patterning in this system is resolved locally and autonomously by neuromast organ precursors. Pattern construction in the medaka pLL is governed by a balance of intrinsic primordium properties and extrinsic influences from its immediate environment, where the modulation of the latter can easily lead to novel pLL patterns. We speculate that this plasticity is exploited evolutionarily to generate novel pLL patterns accommodating the diverse sizes and body-plans of teleost fish.

2. Results

2.1. pLL patterning is unaltered upon pLL nerve ablation

The embryonic pLL pattern construction in medaka involves highly stereotypic organ movements and positioning. Primary neuromasts are deposited by a primordium at the D-V midline (i.e. horizontal myoseptum) along the tail and will end up ventrally, while secondary organs, formed ventrally at later stages, will locate to the midline (Seleit et al., 2017a). We focused on the first step initiating the medaka pLL pattern, i.e. the immediate ventral migration of deposited primary neuromasts. One of the differences between primary and secondary neuromast migration is that primary organs are associated with the pLL nerve when migrating ventrally, while secondary organs migrate dorsally and
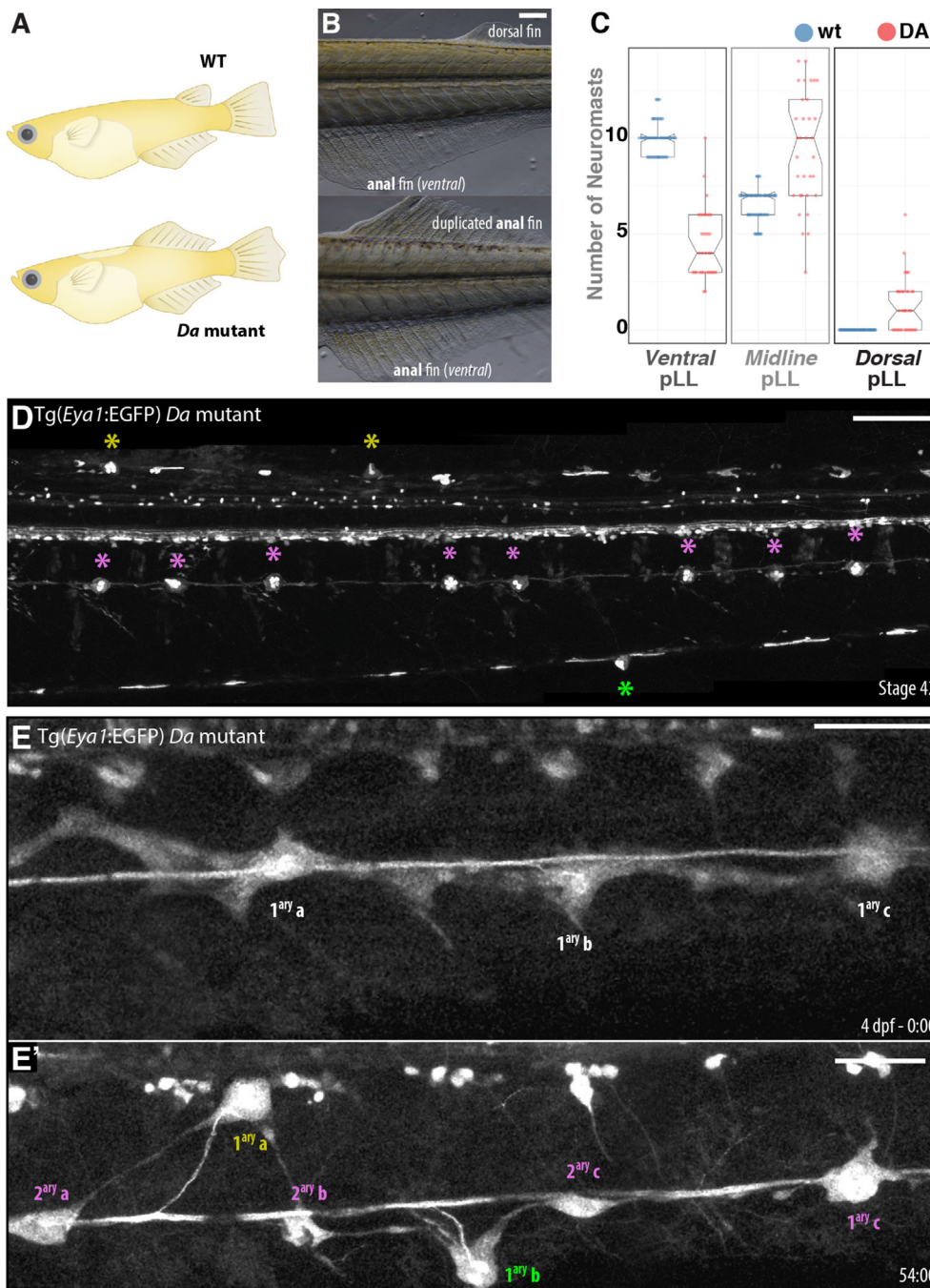

Fig. 3. Location of primary neuromasts in *Da* mutants reveals autonomous organ positioning in the pLL system.

(**A**) Scheme representing main differences in body shapes between adult *wt* and *Da* mutant fish. Notice the duplication of the anal fin dorsally in the *Da* mutant. (**B**) Bright-field view of wt and *Da* medaka larvae showing dorsal and anal fin positions. Scale bar = 100 μm. (**C**) Positioning of embryonic pLL neuromasts in *Da* and *wt* fish. *Da* mutants show a higher number of organs retained at the midline compared to ventral organs. Notice that only the *Da* mutant has neuromasts located on the dorsal side. The variance around the mean is higher in *Da* mutants as compared to *wt* larvae. (**D**) Tg(*Eya1*:GFP) *Da* mutant shows neuromasts located to both ventral and duplicated ventral side (green and yellow asterisks, respectively) while many neuromasts remain stuck in the midline (magenta asterisks). N > 50 Da larvae. Scale bar = 100 μm. (**E-E′**) Snapshots of a 4D-live SPIM imaging on 4 dpf Tg(*Eya1*:GFP) *Da* mutant during pLL organ deposition. Notice primary organs moving to the induced ventral side (yellow label), the regular ventral side (green label) and an organ that remains stuck in the midline (magenta label). Scale bar = 50 μm. Time in hours. N = 5 larvae.

establish pLL nerve connections in their final location (Seleit et al., 2017a). We therefore started by exploring whether the pLL nerve acts instructively to guide primary organs to the ventral side. We decided to target the pLL nerve by two-photon laser ablation and check the resulting pLL pattern, for which we used double Tg(*Eya1*:mCFP, *K15*:H2B-RFP) that guarantees a clear labelling of the pLL nerve and neuromasts (Fig. 2A-A′). We performed a high precision injury to a specific segment of the pLL nerve in 3–4 dpf embryos, when the primordium already deposited a number of primary organs at the midline (Fig. 2B-B″). We were able to leave the primordium, the deposited neuromasts and the un-targeted anterior segment of the pLL nerve intact and uninjured (Fig. 2B″). Interestingly, and contrary to what was reported in zebrafish (Gilmour et al., 2002), the pLL nerve does not regenerate in medaka (N = 11 embryos). Five days post ablation, the analysis of neuromasts distribution in resected embryos revealed a normal pLL patterning despite the loss of the pLL nerve (Fig. 2C, C', N = 11 pLL ablations in 11 embryos) and associated Sox10+ glial cells (Fig. S1). Sox10+ glial cells that are not associated with the pLL nerve, like those running along the vertical myotome boundaries, are not affected by the ablations (Fig. S1). Our results indicate that the pLL nerve is dispensable for correct patterning in the pLL of medaka, raising the possibility that patterning depends on the ability of deposited organs to sense and respond to positional cues.

2.2. pLL patterning is built via the autonomous migration of each neuromast

During pLL formation in medaka, every *primary* neuromast moves ventrally to reach its final location. This can be achieved either by primary neuromasts migrating independently of one another — as *autonomous* units — or alternatively, by a system-level instruction where the entire set of organs responds uniformly — e.g. *collective* migration due to the unfolding of an intrinsic and invariant developmental program. The *Double anal* (*Da*) medaka mutant has a partial duplication of the ventral side along the tail due to the inactivation of *zic* genes (Moriyama et al., 2012; Ohtsuka et al., 2004). This results in a fish with an unperturbed ventral side and a *duplicated* ventral side on the dorsal side of the tail (Fig. 3A and B). The duplication of the ventral side in the *Da* mutant offers the possibility to address whether the pLL pattern arises from a system-level control or from an organ-autonomous response. The system-level organisation would result in all primary organs of a given pLL migrating to the same ventral side – either the *real* ventral or the *duplicated* ventral. In contrast, the organ-independent outcome would result in a pLL harbouring organs located at both ventral sides. The analysis of pLL reporters in Da mutant embryos revealed that 60% of pLLs contained neuromasts at both ventral sides (Fig. 3C and D, compare with wild type pLL in Fig. 1D and E, Fig. 2A, C') (N = 20/33 pLL in 26 medaka *Da*-/-embryos), a phenotype that has never been observed in a wild type embryo (N = 0 in more than 200 pLL in medaka *wt* embryos). Live-imaging on *Da* mutants during pLL pattern construction confirmed that primary organs are autonomous in the direction of their movement even within the same pLL (Fig. 3E, E') (Supplementary Movie 1-2, N = 5 embryos, compare also to Fig. 1C and D). The random migration of primary organs can be explained by either a duplicated expression of an attractant or by the absence of a repressor in the *Da* mutant dorsal domain.

The presence of a pLL nerve reporter in the movies allowed establishing that the pLL nerve connection follows the migratory path of the forming organs irrespective of their migratory direction (Fig. 3E, E'). In addition, we have noticed that in the majority of *Da* mutant pLLs, some primary organs are ectopically located at the midline (Fig. 3C and D)(N = 25/33 pLL in 26 medaka *Da* embryos); 4D imaging revealed that these organ precursors changed their positions multiple times dorsally and ventrally to the horizontal myoseptum before eventually settling at the midline (Supplementary Movie 1-3, N = 5 embryos). Our results indicated that pattern construction in the pLL of medaka is resolved

individually by independent primary organs, most likely depending on their immediate environment. Interestingly, in all cases observed in the *Da* mutant, a secondary organ was formed in between two primaries regardless of their position (ventral-ventral, ventral-dorsal, dorsal-dorsal and dorsal-ventral) (N = 5 embryos) (Supplementary Movie 1). These results point to the fact that intrinsic properties of the pLL (one secondary organ in between two primaries, secondary organ positioning) and extrinsically influenced properties (positioning of primary organs) together govern the construction of the pLL pattern in medaka. Additionally, they highlight the plasticity of this neural system to respond differentially to local changes in its environment on an organ-by-organ level creating novel pLL patterns in the process.

Supplementary video related to this article can be found at https://doi.org/10.1016/j.ydbio.2021.09.002

2.3. pLL patterning is disturbed in siml mutants

Intrigued by the possibility that the immediate environment of the primordium might define the pLL pattern, we decided to disrupt epithelial integrity by targeting *keratin 15 (krt15)* using Crispr/Cas9 (see M&M). We used different combinations of sgRNA against *krt15*, which resulted in F0 crispants and stable mutants (Supplementary Fig. 2) displaying epithelial extrusion (Fig. 4A and B white arrows), perturbations in the structural integrity and cellular packing in the supra-basal epithelial layer (Fig. 4A', B', N > 100 cells segmented in *wt* and mutants, N = 5 control & N =15 mutant larvae), lesions in the basal epithelium (Fig. 4E, N > 10 embryos)(Supplementary Fig. 3) and epithelial cell death (Fig. 4E, E', magenta arrows, N = 5 embryos) as revealed by nuclear rounding and cell membrane shrinkage, all in line with known Krt15 functions in epithelial cells from other systems (Bose et al., 2013; Chamcheu et al., 2011; Giroux et al., 2017, 2018; Haines and Lane, 2012; Liu et al., 2003; Peters et al., 2001). Importantly, crispants and mutants also showed a perturbed pLL pattern, with many primary neuromasts locating to the midline – from here on referred to as *stuck-in-the-midline* or *siml* mutants (Fig. 4C-E'). While primary and secondary organs are arranged in an alternating pattern in *wild types* (N = 24/24 pLLs), we have observed a number of primary organs retained in the midline of *siml* mutants (N = 25/26 *siml* pLLs showing at least one primary organ retained in the midline) (see M&M). A 4D-live imaging approach revealed that a fraction of *siml*-/-primary organs start moving ventrally but are either heavily delayed or blocked from proceeding further, reverting their direction to migrate towards the mid-line. This is also evident by tracing pLL nerve connections, which reflect the path followed by the primary neuromasts until getting their final location (Supplementary Fig. 4).

The 4D imaging on *siml*-/- mutants also revealed that primordium migration is significantly slower and stuttered as compared to control embryos (4,71 ± 2,38 µm/h in *siml* mutants, N = 3 embryos; 17,95 ± 3,69 µm/h in *wild types,* N = 5 embryos) (Supplementary Movies 4-5, N = 3 *siml* mutant fish, 3 *wt* fish and 3 Da mutant fish). Stuttering of the primordium coincides with the presence of epithelial lesions that block the path through the epithelium (Supplementary Movies 4-5). In a scenario where the pLL primordium is migrating slower, it has to be considered whether primordium speed impacts the final position of primary organs in *siml*-/- mutants. Two observations argue against this reasoning. First, *kazoura* mutants in medaka (*cxcr4b*-/-) display a slow-migrating pLL primordium (9,35 ± 0,76 µm/h, N = 3 embryos) (Seleit et al., 2017a) and primary neuromasts still migrate ventrally immediately after deposition. Second, *Da*-/- mutants display a pLL primordium that migrates similar to the *wt* speed (18,28 ± 4,71 µm/h), and we can observe a big proportion of embryos in which primary neuromasts locate to the midline (N = 25/33 pLL in 26 medaka *Da* embryos). Therefore, the final position of primary organs does not correlate to the speed of pLL primordium migration. Intriguingly and regardless of the abnormal location of primary neuromasts in *siml* mutants, secondary organs form in between primary organs and locate properly to the midline. This indicates
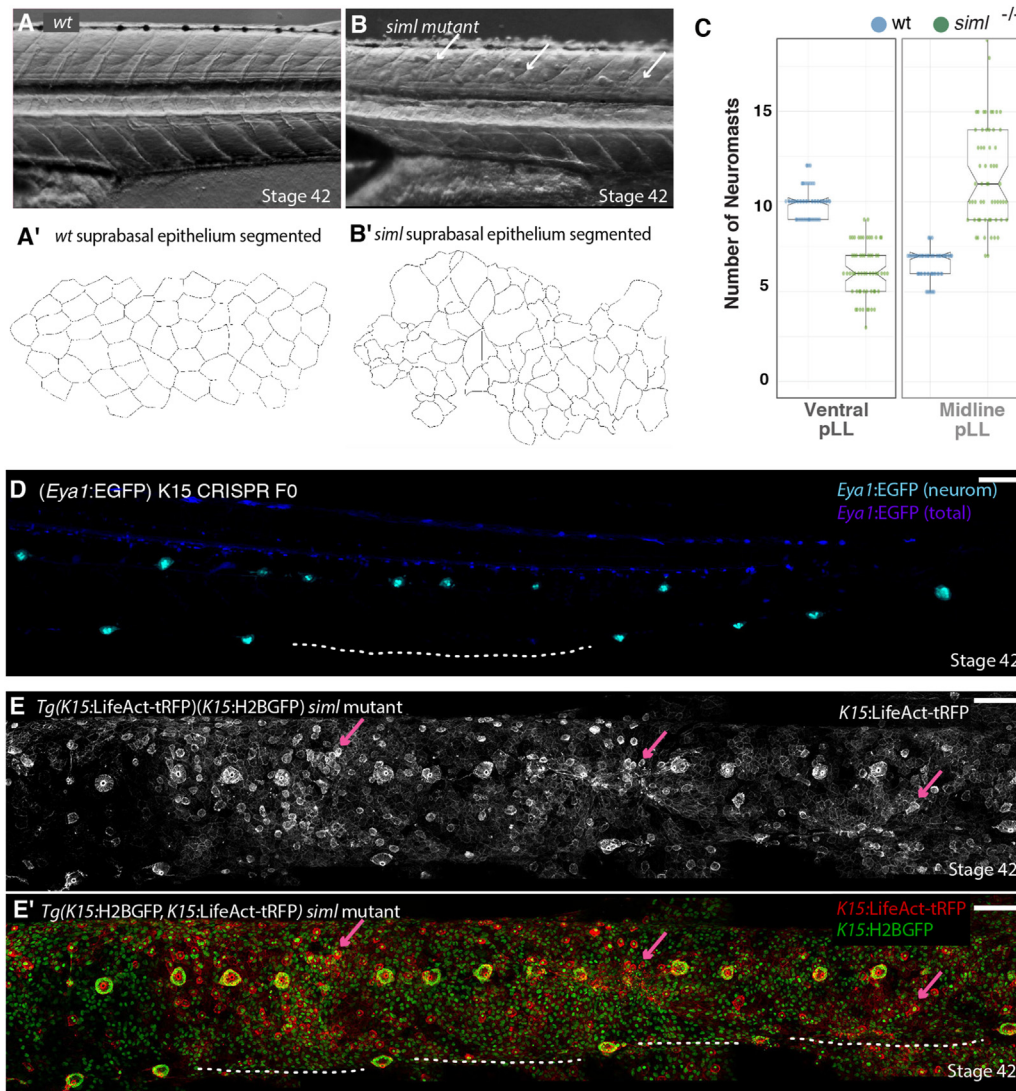
Fig. 4. *siml* mutants show epithelial and pLL patterning defects.

(**A-B′**) Bright-field imaging of wt (A) and *siml* (B) stage 42 larva, and manual segmentation of suprabasal epidermis in wt (A′) and *siml* mutant (B′). Notice the presence of extruding cells from the epithelial cell layer (B, white arrows) and the massive disorganisation, loss of structural packing and loss of uniform cell size (B′). N > 100 cells segmented in *wt* and *siml* mutants, N = 5 control & 15 *siml* mutant larvae. (**C**) Distribution of embryonic pLL neuromasts in wt and *siml* mutants larvae, notice the inversion of midline vs ventral neuromasts in the *siml* mutants compared to *wt*. The variance around the mean is higher in *siml* mutants than wt fish. (**D**) Confocal image of a Tg(*Eya1*:EGFP) injected with Cas9 + gRNA1,2 against *krt15* locus. Whole EGFP expression is in blue and neuromasts are displayed in green to highlight pLL. N > 100 injected embryos, 40% showing a phenotype in pLL patterning (notice the ventral regions devoid of primary neuromasts, white dotted line) and skin lesions. (**E-E′**) Confocal image of a double Tg(*K15*:H2B-GFP)(*K15*:LifeAct-tRFP) *siml* mutant (E, Life-Act-RFP, E′, merge). Notice the presence of epithelial lesions (magenta arrows) and the heavily perturbed pLL pattern (E′) where many primary neuromasts are located at the midline (ventral regions devoted of primary neuromasts are indicated by a white dotted line). Scale bar = 100 μm.

once again that both the appearance of a secondary organ between 2 consecutive primary neuromasts and the position of secondary organs along the horizontal myoseptum are indeed intrinsic features of the pLL system. Overall, our data reveals a rationale where the location of primary neuromasts is plastic, while the formation of secondary neuromasts and their position is a fixed property of the pLL system.

Supplementary video related to this article can be found at https://doi.org/10.1016/j.ydbio.2021.09.002

2.4. pLL patterning depends on local epithelial cell integrity

We have previously shown that *keratin 15* is expressed in mature neuromasts, particularly in the mantle cells – the neural stem cells of the pLL system (Seleit et al., 2017b). To check whether *krt15* was expressed at earlier stages within the primordium, we performed a double *in situ* hybridisation using *eya1* and *krt15* specific probes. This showed that *krt15* mRNA is not detectable in the primordium during migration stages (Fig. 5A-B″ N = 3), indicating that the pLL patterning defect observed in the *siml* mutant might indeed originate extrinsic to the primordium. Since we have previously shown that the neuromasts and their surrounding epithelium have two independent embryonic origins in medaka, we decided to perform blastula stage transplantation assays from *siml* mutants into *wt* and vice-versa (Seleit et al., 2017b). This will reveal whether the patterning defects in the *siml* mutant arise intrinsically due to defects

in the primordium or extrinsically from the local environment the primordium travels through. Our results show that the presence of a large majority of *siml* mutant cells within a primary neuromast does not lead to any patterning defects (Fig. 6A-B″, n = 12 mosaic neuromasts in N = 6 chimeric embryos), since neuromasts correctly position to the ventral side and the pLL pattern observed is equivalent to the *wild-type*. On the other hand, the presence of a vast majority of *wild type* cells in the neuromast of a *siml* mutant larva fails to rescue the pLL patterning defect (Fig. 6C, D, n = 6 mosaic neuromasts in N = 3 chimeric embryos). As an extreme example, we obtained a transplanted fish in which *wild type* cells contributed to the epidermis of the right side of the tail in an otherwise *siml* mutant background. In that larva, the left pLL displayed the typical aberrant organ distribution reported for *siml*, with most neuromasts located along the midline (Fig. 6E-E″). On the right side, however, the presence of a *wild type* epidermis rescued the alternating distribution of neuromasts, where primary organs locate ventrally and secondary neuromasts locate at the middle (Fig. 6F-F″). These data combined with previous results strongly argue that the observed pLL patterning defect in *siml* mutants arises from the local environment through which the primordium and primary deposited organs migrate, namely the epidermis.

Complementing the genetic perturbation of the *keratin 15* locus, we decided to mechanically interfere with epithelial cell integrity, to address whether the disruption of the epidermis was the driving force behind the aberrant neuromast distribution in *siml* mutants. Using 2-photon laser
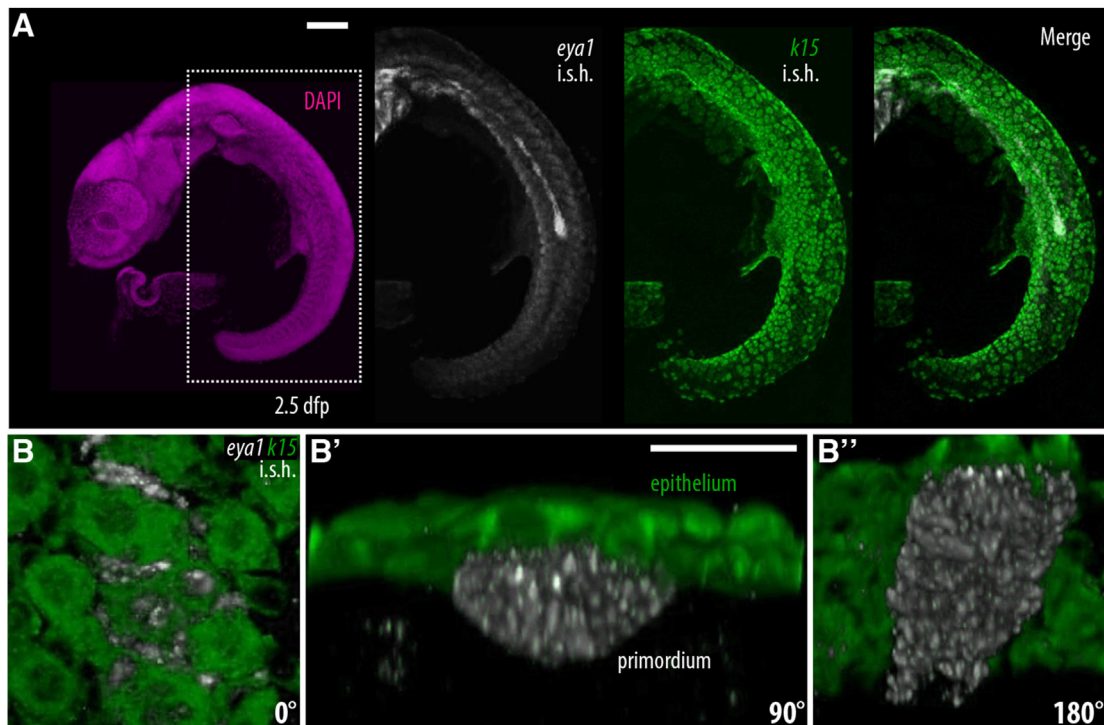
Fig. 5. *krt15* is expressed by cell in the epidermis but not detected in the migrating pLL primordium.
(**A**) Double *in situ* hybridization using *eya1* and *krt15* antisense probes during primordium migration stage. *eya1* is strongly expressed in the primordium while *krt15* is mainly in the epidermis with no detectable expression in the primordium. Scale Bar = 100 μm. (**B–B″**) 3D reconstruction on the primordium of a sample treated as in (A). 0°, 90°, and 180° rotations to show differential expression of *eya1* in the primordium and *krt15* in the epidermis. Scale bar = 20 μm.

ablation we targeted *krt15* positive epithelial cells directly ventral to deposited primary organs during primordium migration in 3–4 dpf *Krt15*:mYFP embryos (Fig. 7A), leaving both the primordium and deposited organs uninjured and intact. Indeed, the pLL primordium in treated embryos was in every case capable of reaching the caudal fin while depositing neuromasts in its way (N = 5). Iterative imaging 48 h post ablation revealed that mechanically-induced lesions interfered locally with correct ventral migration of primary organs recapitulating our results from the *siml* mutant (Fig. 7B-C', N = 5 ablated embryos and N = 3 non-ablated controls). Notably, neuromasts anterior and posterior to the injury site, not exposed to a mechanical perturbation in their immediate surrounding, positioned correctly along the body axis (Fig. 7C). Importantly, by 48 h post ablation the skin injury is repaired yet targeted neuromasts do not proceed to locate ventrally, this rules out that primary neuromast positioning is a purely cell intrinsic property. Overall, our results indicate that the pLL pattern is easily modulated by changes in tissues external to the primordium (*i.e* the epidermis), suggesting that this adaptability can be exploited evolutionarily to match a somatotopic sensory system to variable body shapes.

3. Discussion

How biological patterns are built and how they evolve is a central question in developmental biology. It is still unclear how reproducibility within one species is balanced with the requirements of evolution of forms and patterns between species. A kaleidoscopic diversity of body plans exists in teleost fish (Coombs et al., 1988, 2014), this raises immediate problems for the set-up of a peripheral nervous system component like the neuromasts of the lateral line (Ghysen and Dambly-Chaudiere, 2016). On the one hand the system must be tunable and easily adjustable to fit the diverse body plans of the different species, and on the other it must still be reproducible within and between members of the same species. In this work we show a strategy that relies on balancing the strict internal properties of the system (*reproducibility*)

with a plastic response to the immediate microenvironment (*adaptability*). Our results show that a new pattern can be obtained without changing any internal or genetic properties of the cells executing organogenesis. Instead, the system has the capacity to sense, react and respond to changes in its surroundings in an organ autonomous manner. That these changes happen during embryogenesis emphasises the already well-established paradigm of development as the playing field of evolution (Carroll, 2005). The self-organizing and hierarchical nature of the process ensures that small changes in conditions can lead to large variations in patterns without affecting organ morphogenesis. By probing differential organ positioning the pLL system is well suited for a rapid evolutionary diversification; indeed, by looking at different embryonic pLL patterns in a number of species we were able to see evidence of this plasticity at play (Fig. 8).

An unexpected outcome of the nerve ablation experiments is the observation that medaka pLL nerve is not able to re-grow after injury, a situation that differs from what is reported in zebrafish (Gilmour et al., 2002). This deficiency in regenerative potential in medaka has been reported for a number of other organs (Ito et al., 2014; Lai et al., 2017; Lust and Wittbrodt, 2018) and the peripheral nervous system can now be added to the growing list of regeneration-deficient components. The molecular underpinnings of this fundamental difference in regenerative capacities between different teleosts is only beginning to be explored (Lai et al., 2017; Lust and Wittbrodt, 2018). Lastly, it has been previously reported in zebrafish that peripheral nerves act instructively during post-embryonic neuromast formation (Wada et al., 2013b), since organs will not form without a preceding nerve outgrowth. In the embryonic pLL development in medaka, however, the nerve is entirely dispensable for organ formation, organ numbers and pLL patterns, highlighting that even within similar systems, the hierarchical logic governing the sequence of events required for their construction can be markedly different.

In medaka, neuromasts in the pLL invariably alternate between the midline and ventral lines. This holds true irrespective of the total number of organs that the posterior lateral line harbours, demonstrating the
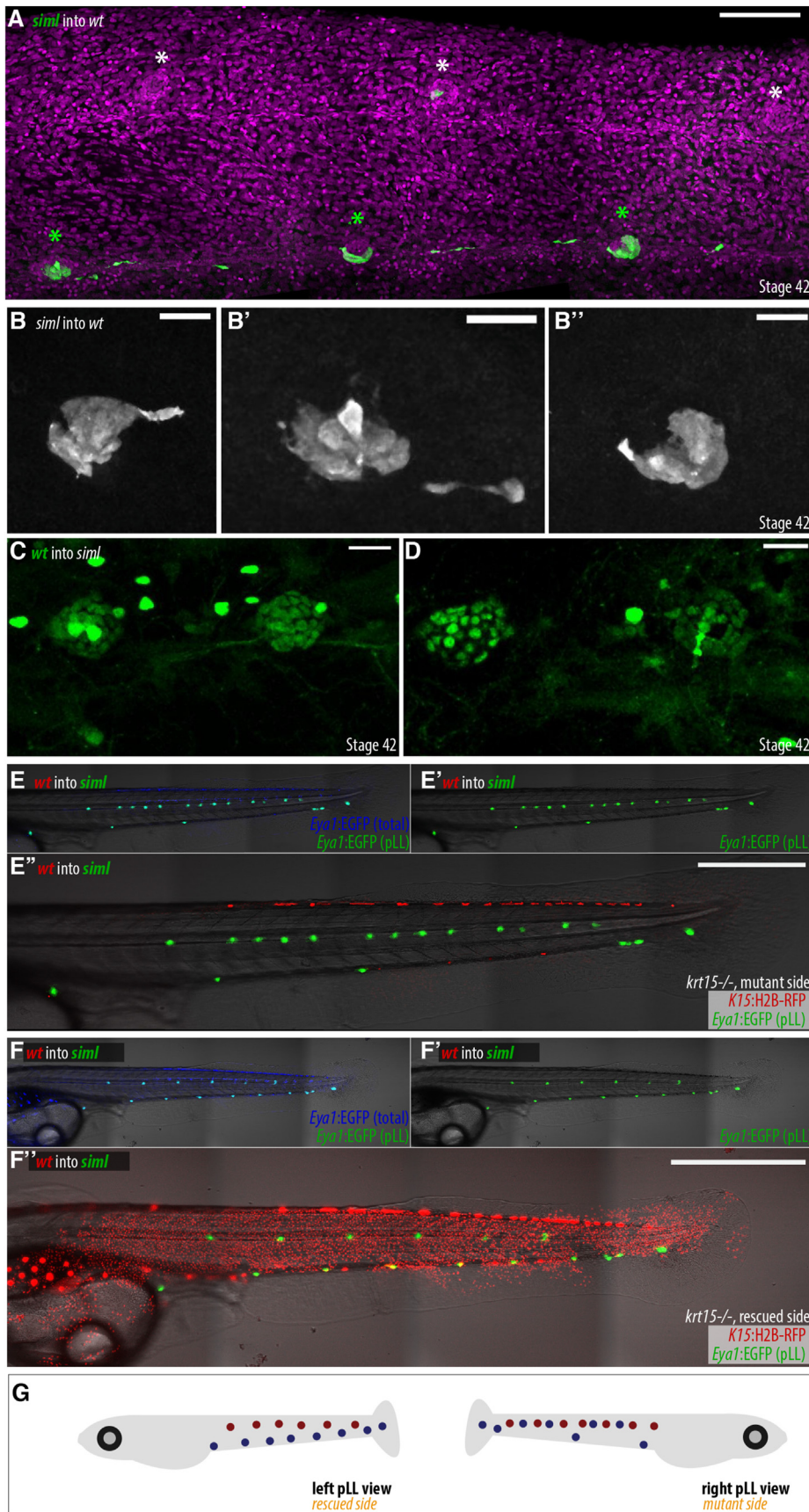
Fig. 6. Perturbed *siml* mutant epidermis causes pLL patterning defect.

(**A-B″**) Anti-EGFP antibody staining on chimeric larvae where Tg(*Eya1*:GFP) *siml* mutant cells were transplanted into unlabelled *wild-type* background. (A) Organs with majority of *siml* mutant cells position correctly to the ventral side. N = 6 transplanted embryos, n = 12 mosaic organs. Scale bar = 100 μm. (B–B″) Close up on ventral mosaic organs showing majority of *siml* mutant cells. Scale bar = 20 μm. (**C-D**) In vivo imaging of chimeric larvae where Gaudi^{LoxPOUT} donor cells (ubiquitously expressing H2B-EGFP) were transplanted into unlabelled *siml* mutants. Even the organs containing mostly *wild type* cells remain at the midline. N = 3 transplanted fish and n = 6 neuromasts. Scale bar = 20 μm. (**E-F″**) A chimeric *siml* mutant larvae that displays wild type cells in the epidermis along the right trunk rescues the alternating distribution of neuromasts. EGFP expression in Tg(*Eya1*:EGFP) is displayed in blue (E, F), while EGFP positive neuromasts are represented in green (a subgroup of EGFP positive cells)(E′, E″, F′, F″). The *siml* mutant side (E″) shows the aberrant neuromast location. *siml* mutant neuromasts arrange in an alternating manner (F″) when surrounded by wild type epithelial cells (red). (G) Scheme of the left (rescued) and right (mutant) pLL system in the mosaic fish displayed in E-F″. Scale bar in E″, F″ = 1 mm.
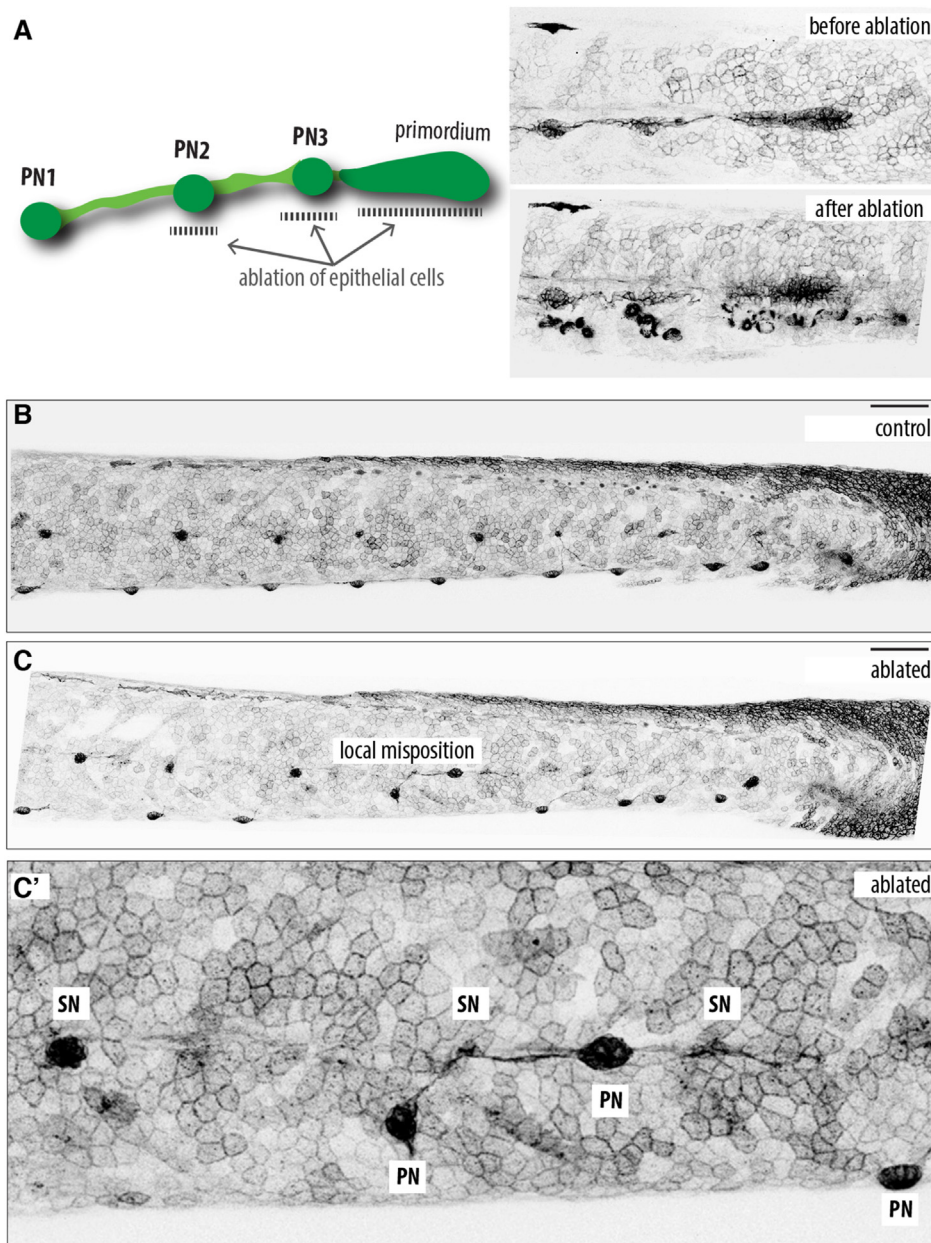
Fig. 7. Local mechanical perturbation of epidermis leads to pLL patterning defects.
(**A**) Schematic diagram of 2-photon ablation on Tg(*K15*:mYFP), 3 dpf. (left). Tg(*K15*:mYFP) embryos showing primordium migration and primary deposited organs before (upper right) and immediately after (bottom right) 2-photon laser ablation of epithelial cells below primary deposited organs. (**B**) A 5 dpf. control, unablated Tg(*K15*:mYFP) showing alternating neuromast pattern with primary organs locating ventrally. (**C**) 48 h post epithelial cell ablation, two primary organs fail to migrate ventrally at the site of injury, while organs anterior and posterior to the injury site locate normally. (**C′**) Close up view of primary organs that failed to migrate ventrally in (C). N = 5 ablated fish and 3 controls. Scale bar = 100 μm.

robustness of the pattern accommodating variable organ numbers (Seleit et al., 2017a). By challenging the medaka lateral system to different contexts we were able to gain new insights into the operational logic behind pLL pattern construction. The *Da* mutant challenges the system by the presence of two ventral sides on the tail, revealing the autonomous nature of organ positioning, *i.e.* primary neuromasts locate to the ventral, dorsal (*induced ventral*) or midline independently of one another. Organ positioning is therefore resolved in a neuromast neighbour-independent manner arguing against the presence of a system level control on the process. We report that the generation of a secondary organ between two primaries is an *intrinsic* property of the medaka pLL primordium, observed in the *Da* mutant, the *siml* mutant and in the ablation of the pLL nerve. However, our combined data rules out the possibility that pLL patterning of medaka is a purely intrinsic property. *Extrinsically*, the immediate environment the primary deposited organs travel through directly influences their final position and therefore the overall pLL pattern at the end of embryogenesis. The same extrinsic logic was recently reported in zebrafish for an earlier step in pLL formation, where

researchers establish the epithelium as a necessary tissue for primordium migration (Nogare et al., 2019).

Additionally, we observe that even within the same larvae – wild type, *Da* or *siml* – the distribution and/or number of neuromasts can be decoupled between the left and the right pLLs (5/7 larvae for Da and 5/13 larvae for *siml*). Both the asymmetries in organ distribution between left and right pLLs within a fish, and the fact that some but not all primary organs are mislocated along a given mutant pLL, strongly suggests that non-genetic causes, like local interactions, might contribute to the phenotypic plasticity of pLL patterning. Our results point to a high potential of plasticity in the system but within defined and strict boundaries ensuring a reproducible outcome. A sequential order emanates from the interplay of *intrinsic & extrinsic* controls, where: first, local extrinsic parameters modulate primary organ positioning; second, neuromast migration dictates the innervation and therefore neuronal network (Haas and Gilmour, 2006); and third, the final position of the organ induces *in situ* the formation of a life-long niche for neuromast stem cells during organ maturation (Seleit et al., 2017b). The same hierarchical
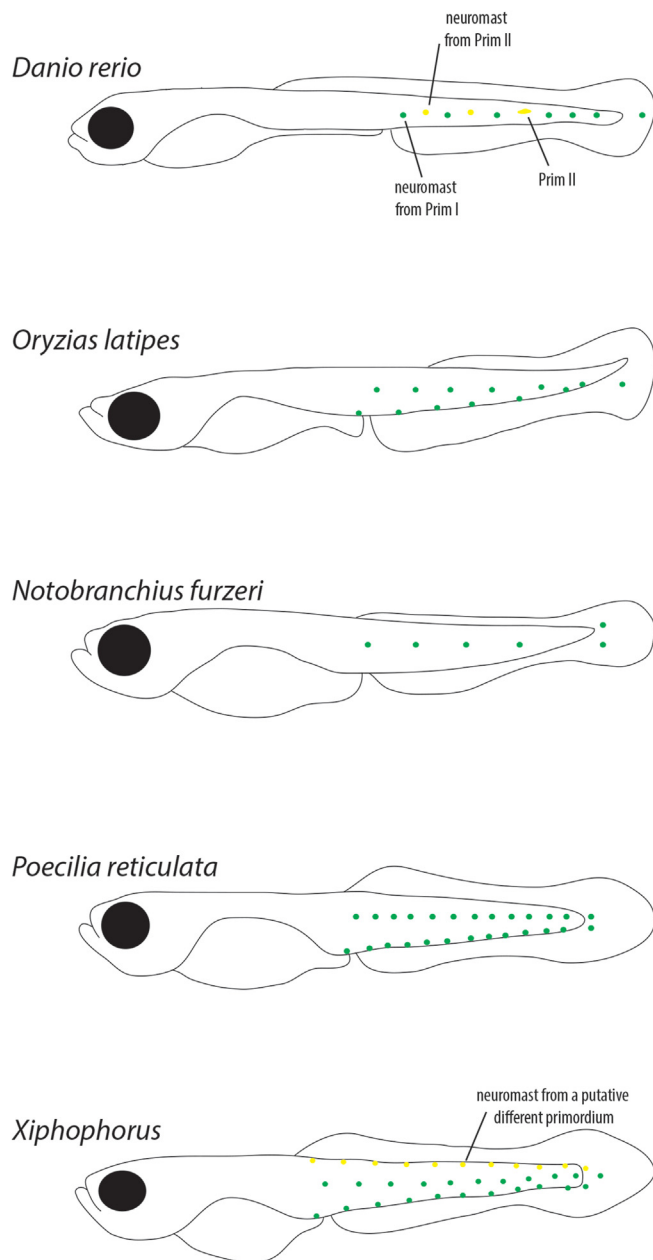
Fig. 8. Diversity of embryonic pLL pattern and organ number in different teleosts.
The diversity of pLL patterns at the end of embryogenesis in a variety of teleosts. Scheme showing the distribution and approximated organ numbers in a variety of teleost fish that were stained using either DAPI or DiAsp and imaged. N = 4 for each species, but zebrafish and medaka N > 20. Fish embryos are not drawn to scale.

organisation is well reported in different induction paradigms, like the induction of the lens by the neural retina in vertebrates (Cvekl and Ashery-Padan, 2014) or the generation of a new neural plate by the Henses' node in chicken (Storey et al., 1992) (Anderson and Stern, 2016).

3.1. The pLL as a system with a low developmental buffering capacity

While both *siml* and *Da* mutants result in a majority of organs retained at the midline, the phenotypes and their aetiology are distinct. Firstly, in *Da* mutants some organs end up in the dorsal side, an outcome never observed in the *siml* mutants nor in the wild type. Secondly, long-term live imaging on both mutants revealed that the way the phenotype

manifests itself is entirely different. On the one hand organs continually move above and below the horizontal myoseptum in the *Da* mutants in a tug-of-war over positioning that results in some organs locating to the ventral side, some dorsally and others retained at the midline. On the other hand, all organs are specified correctly in *siml* mutants and start to move ventrally, some are stopped from proceeding further and revert to the midline. Our results argue that distinct mechanisms cause the *Da* and *siml* phenotypes, and while primary organs can be retained at the midline in both mutants the reasons for that outcome are entirely different. The convergence of different mutants to the same distribution of pLL neuromasts in the myoseptum, suggests that *neuromasts-in-the-midline* is a phenotypic node of the system.

Recent work has argued for cis-regulatory element refurbishment as a means for evolutionary tinkering (Chan et al., 2010; Indjeian et al., 2016; Jones et al., 2012; McLean et al., 2011; O'Brown et al., 2015; Prud'homme et al., 2006). Our data support the hypothesis that for the lateral line sensory system, these changes do not need to occur within the pLL founding tissue *per se* and do not need to involve any regulatory changes within the genetic landscape controlling primordium migration. The unpredictability of individual organ positioning in *Da* and *siml* mutants points towards the fact that the posterior lateral line system is phenotypically plastic or has a low developmental buffering capacity (Waddington, 1959, 1968, 1969). The concept of developmental buffering was first described by Conrad Waddington to explain the canalization of developmental processes i.e. the arrival at the same reproducible outcome despite small genetic and non-genetic differences in starting conditions (Waddington, 1941, 1959, 1968, 1969). However, it was also recognised that different developmental modules must have different buffering capacities depending on need (Waddington, 1959). In the case of the pLL it would be evolutionarily beneficial to operate under a low developmental buffering capacity as it would make the system highly susceptible to small changes in conditions, i.e. the shape of the tail in different teleost species. It is tempting to speculate that the high plasticity of the system could be exploited evolutionarily to generate diverse patterns of lateral lines in the wild – like the ones observed between surface and cave-fish (Sumi et al., 2015), or between salt and fresh water conditions in sticklebacks (Wark and Peichel, 2010). Combining examples from the literature and our own cross-species observations confirms that embryonic pLL patterns are variable among different teleost species (Fig. 8), highlighting once more the degree of plasticity and fast evolvability of this developmental module.

4. Materials and methods

4.1. Animal strains used

Medaka were maintained as closed stocks at the Centre of Organismal Studies of the University of Heidelberg (Tierschutzgesetz §11, Abs. 1, Nr. 1). The fish colony was maintained under standard recirculating aquaculture conditions, 14 h of light and 10 h of darkness. The strains used in this study are: *Cab* (wild-type population), *Da* mutant (Ohtsuka et al., 2004).

4.2. Transgenic lines

We have used the following transgenic lines: Tg(*Eya1*:mECFP), Tg(*Eya1*:EGFP), Tg(*K15*:H2B-EGFP), Tg(*K15*:H2B-RFP) (Seleit et al., 2017a, 2017b), *Gaudi*^LoxPOUT (Centanin et al., 2014). The newly generated transgenic lines are:

Tg(*Sox10*:mCherry): The plasmid *sox10*:mCherry (a gift from Thomas Look, Addgene plasmid # 98695) was injected in wild type or *Da-/-* medaka embryos at the one cell stage using I-SceI meganuclease protocols as previously described (Thermes et al., 2002).

Tg(*K15*:LifeAct-tRFP): A LifeAct-tRFP peptide was clone under the previously published medaka *krt15* partial promoter (Seleit et al., 2017b) using Age1 and Not1 restriction enzymes. The resulting plasmid

K15:LifeAct-tRFP was injected in medaka embryos at the one cell stage.

4.3. Generation of siml mutants

Two gRNAs targeting exons of *keratin 15* were designed using CCTop (Stemmer et al., 2015) and synthesised as previously described (Stemmer et al., 2015). The sequences of *krt15* gRNAs are UGACCGGCUUGCCAG-CUACCUGG and CACUGGUCAGGUCAACGUUGAGG. The following oligos were used:

sgRNA-1_F: TAGGTGACCGGCTTGCCAGCTACC
sgRNA1_R: AAACGGTAGCTGGCAAGCCGGTCA
sgRNA-2_F: TAGGCACTGGTCAGGTCAACGTTG
sgRNA-2_R: AAACCAACGTTGACCTGACCAGTG.

Annealed oligos were ligated into linearised DR274 plasmids (Addgene clone number: #42250) as described before (Seleit et al., 2017b). This was followed by *in vitro* RNA transcription using T7 MEGAshortscript Kit (Ambion) and cleaned-up using RNAeasy kit (Qiagen). The gRNAs were co-injected at 15 ng/µl each along with 150 ng/µl of CAS9 mRNA into Tg(*Eya1*:EGFP), Tg(*Eya1*:mCFP), Tg(*K15*:H2BGFP), Tg(*K15*:LifeActtRFP) and *wild type* one-cell-stage medaka embryos. To check for gRNA efficiency the following genotyping primers were used: *krt15* fwd, GGGACCA-GAGTCTCTGTTTCC, *krt15* rev, TTGGTGTTCCATGTCGTTGC. Crispants resulting from the injection of either gRNA 1, gRNA2 or gRNA1+gRNA2 into the different genetic backgrounds showed the same, reproducible phenotypes with high penetrance. The phenotypes (disruption of the epithelium, pLL neuromasts stuck in the midline, referred to as *siml*) were displayed by F1 and F2 mutants, generated through in-crosses of the previous generations. Individual adults of the F2 mutant lines were genotyped by PCR using *krt15 fwd* and *krt15 rev* primers, and the amplicons were analysed by Sanger sequencing. We identified several alleles, from which we selected the ones described in Supplementary Fig. 1 to grow allelic series by out-crosses to wild type fish. We have noticed that in later generations (from F4 on) the penetrance of the phenotypes decreased, obtaining in cases stocks of *keratin 15* mutants in which the phenotype was absent. In every case, though, when *krt15*/+ adults were incrossed and their progeny was sorted for the *siml* phenotype, a genotyping PCR confirm that *siml* fish were indeed *krt15*^{D594} Homozygous mutants (15/16 *krt15*^{D594} homozygous, 1/16 *krt15*^{D594} heterozygous).

4.4. Transplantation assay

Blastula stage transplantations in medaka were carried out as previously described (Rembold et al., 2006). Briefly 10–35 cells were transplanted from *Gaudi*^{LoxPOUT} (ubiquitously expressing H2B-GFP), or (*K15*:H2B-RFP) donors into *siml* mutant hosts, and from *siml* mutant donors (*Eya1*:GFP and *K15*:H2BGFP) into wt hosts. Transplanted embryos were kept in 1 × ERM supplemented with antibiotics (penicillin-streptomycin solution from Sigma, P0781) and selected for fluorescent expression in the primordium. Positively transplanted fish with labelled donor cells in the neuromasts or in the vicinity of the neuromasts were analysed at stage 42 under a fluorescent binocular or under a confocal microscope.

4.5. Live-imaging and sample preparation

For dechorionisation, embryos were rolled on commercially available sand-paper, washed in 1 X ERM, treated with hatching enzyme for 30–50 min at 28 °C, and washed abundantly in ERM to remove any residual enzyme. All live-imaging was done as previously described (Seleit et al., 2017a, b). Briefly, dechorionated embryos or hatchlings were anaesthetised in 1x ERM supplemented with Tricaine (Sigma-Aldrich, A5040) and then mounted in 0.6% low melting agarose on glass bottom dishes (MatTek corporation). Embryo screening was performed using either the Olympus MVX10 macrofluorescence binocular. Live-imaging was done using the MuVi-SPIM (Krzic et al., 2012) with two illumination objectives (10x Nikon Plan Fluorite Objective, 0.30 NA) and two

detection objectives (16X Nikon CFI LWD Plan Fluorite Objective, 0.80 NA). Additional live-imaging was done using the confocal laser-scanning microscope Leica TCS SPE (40x oil objective) or Leica TCS SP5 II (10X dry, 40x dH$_2$O objectives). Samples were placed in the Microscope Slide Temperature Controller from Biotronix to control temperature.

4.6. Image and data analysis

All Image analysis was done using FIJI and ImageJ. Image stitching utilized 2D and 3D stitching plug-ins on ImageJ. All registration of imaging time-stamping, manual tracking, and manual segmentation of cells, was done using standard FIJI plug-ins.

4.7. Stainings

Immunohistochemistry: IHC were performed on fixed medaka embryos as described before (Centanin et al., 2014). Primary antibodies used were Anti-eGFP Rabbit (Invitrogen, 1:500) and anti-tRFP Rabbit (Evrogen, 1:250). Secondary antibodies used were goat anti-Rabbit Alexa Fluor 488 (Invitrogen, 1:500), goat anti-Rabbit Alexa Fluor 546 (Invitrogen, 1:500). For DAPI staining a final concentration of 5 ug/l was used.

Double *in situ* Hybridisation: Samples were prepared as previously described (Seleit et al., 2017a). Hybridisation was performed with the *eya1* (DIG) and *krt15* (Fluo) probes in hybridisation mix overnight at 65 °C. All following washing steps were done with TNT (0.1M Tris pH 7.5, 0.15M NaCl, 0.1% Tween20). The samples were blocked in 2% TNB (2% blocking reagent (Roche, REF 11 096 176 001) in TNT for 2–3 h at room temperature and incubated with an anti-Fluo-POD antibody (1/50, Sigma-Aldrich REF 11 426 346 910) in 2% TNB overnight at 4 °C. On the next day after washing detection of the *krt15* probe was performed using the PerkinElmer TSATM-Plus Fluorescein System (NEL741B001KT). To stop all remaining POD enzyme activity the samples were incubated 20 min in 2% H2O2 in TNT. For visualization of the *eya1* probe the samples were incubated with an anti-Dig-POD antibody (1/50 in 2% TNB, Sigma-Aldrich REF 11 207 733 910) and DAPI (1/1000) overnight at 4 °C. Detection of the *eya1* probe was performed using the PerkinElmer TSATM-Plus Cyanine 3 System (NEL744B001KT). The embryos were mounted in 0.6% low melting agarose in PTW and imaged at a confocal microscope.

DiAsp: Hair cells in neuromasts were visualised using the vital dye 4-Di-2-ASP (Sigma-Aldrich) as previously described (Sapède et al., 2002; Seleit et al., 2017a). Live samples were incubated for 5–10 min in a 5 mM DiAsp solution, washed in ERM and analysed using a fluorescent binocular.

4.8. 2-Photon laser ablation

For pLL nerve ablations a multi-photon laser coupled to a Leica TCS SP5 II microscope was used. Conditions varied across the replicates, the 'point ablation' function was utilized using 880 nm wavelength and a laser power between 30 and 50% for a timeframe of 300–800 ms. A section of the pLL nerve was chosen and from 6 to 20 sequential points were ablated. Directly after injury the pLL nerve was imaged to check the efficiency of targeting the nerve. In other experiments, we targeted 5–15 EYFP positive epithelial cell membranes underneath the primordium and latest deposited neuromasts in Tg(*K15*:mEYFP) 3–4 dpf embryos during pLL pattern construction. Point ablation settings were used and laser power varied between 30 and 52% with a time frame of 200–300 ms. Embryos were imaged before and after to check the success of targeting.

5. Ethics approval and consent to participate

Medaka and zebrafish husbandry and experiments were performed according to local animal welfare standards (Tierschutzgesetz 111, Abs. 1, Nr. 1, Haltungserlaubnis) and in accordance with European Union

animal welfare guidelines. The fish facility is under the supervision of the local representative of the animal welfare agency.

Consent for publication

Not applicable.

Availability of data and materials

All data generated or analysed during this study are included in this published article [and its supplementary information files].

Funding

Authors' contributions

AS, Conceptualization, Validation, Formal analysis, Investigation, Writing – original draft preparation, Writing – review and editing, Visualization. KG, Validation, Formal analysis, Investigation, Writing – review and editing, Visualization. JO, Validation, Formal analysis, Investigation, Writing – review and editing, Visualization. OPH, Validation, Investigation. JT, Validation, Investigation. LC, Conceptualization, Validation, Formal analysis, Investigation, Writing – original draft preparation, Writing – review and editing, Visualization, Supervision, Project administration, Funding acquisition.

Declaration of competing interest

The authors declare that they have no competing interests.

Acknowledgements

Appendix A. Supplementary data

Supplementary data to this article can be found online at https://doi.org/10.1016/j.ydbio.2021.09.002.

References

Aman, A., Piotrowski, T., 2008. Wnt/β-Catenin and Fgf signaling control collective cell migration by restricting chemokine receptor expression. Dev. Cell 15 (5), 749–761.

Anderson, C., Stern, C.D., 2016. Organizers in development. Curr. Top. Dev. Biol. 117, 435–454.

Bose, A., Teh, M.T., Mackenzie, I.C., Waseem, A., 2013. Keratin k15 as a biomarker of epidermal stem cells. Int. J. Mol. Sci. 14 (10), 19385–19398.

Carroll, S.B., 2005. Endless Forms Most Beautiful : the New Science of Evo Devo and the Making of the Animal Kingdom, first ed. ed. Norton, New York, p. 350. xi.

Centanin, L., Ander, J.-J., Hoeckendorf, B., Lust, K., Kellner, T., Kraemer, I., et al., 2014. Exclusive multipotency and preferential asymmetric divisions in post-embryonic neural stem cells of the fish retina. Development 141 (18), 3472–3482.

Chamcheu, J.C., Siddiqui, I.A., Syed, D.N., Adhami, V.M., Liovic, M., Mukhtar, H., 2011. Keratin gene mutations in disorders of human skin and its appendages. Arch. Biochem. Biophys. 508 (2), 123–137.

Chan, Y.F., Marks, M.E., Jones, F.C., Villarreal Jr., G., Shapiro, M.D., Brady, S.D., et al., 2010. Adaptive evolution of pelvic reduction in sticklebacks by recurrent deletion of a Pitx1 enhancer. Science 327 (5963), 302–305.

Chitnis, A.B., Nogare, D.D., Matsuda, M., 2012. Building the posterior lateral line system in zebrafish. Dev. Neurobiol. 72 (3), 234–255.

Coombs, S., Janssen, J., Webb, J.F., 1988. Diversity of lateral line systems: evolutionary and functional considerations. In: Atema, J., Fay, R.R., Popper, A.N., Tavolga, W.N. (Eds.), Sensory Biology of Aquatic Animals. Springer New York, New York, NY, pp. 553–593.

Coombs, S., Bleckmann, H., Fay, R.R., Popper, A.N. (Eds.), 2014. The Lateral Line System. Springer, New York, NY. New York.

Cvekl, A., Ashery-Padan, R., 2014. The cellular and molecular mechanisms of vertebrate lens development. Development 141 (23), 4432–4447.

David, N.B., Sapède, D., Saint-Etienne, L., Thisse, C., Thisse, B., Dambly-Chaudière, C., et al., 2002. Molecular basis of cell migration in the fish lateral line: role of the chemokine receptor CXCR4 and of its ligand, SDF1. Proc. Natl. Acad. Sci. U. S. A 99 (25), 16297–16302.

Eiraku, M., Takata, N., Ishibashi, H., Kawada, M., Sakakura, E., Okuda, S., et al., 2011. Self-organizing optic-cup morphogenesis in three-dimensional culture. Nature 472 (7341), 51–56.

Ghysen, A., Dambly-Chaudière, C., 2007. The lateral line microcosmos. Gene Dev. 21 (17), 2118–2130.

Ghysen, A., Dambly-Chaudiere, C., 2016. Development vs. behavior: a role for neural adaptation in evolution? Int. J. Dev. Biol. 60 (4–6), 77–84.

Ghysen, A., Schuster, K., Coves, D., de la Gandara, F., Papandroulakis, N., Ortega, A., 2010. Development of the posterior lateral line system in Thunnus thynnus, the Atlantic blue-fin tuna, and in its close relative Sarda sarda. Int. J. Dev. Biol. 54 (8–9), 1317–1322.

Ghysen, A., Dambly-Chaudière, C., Coves, D., de la Gandara, F., Ortega, A., 2012. Developmental origin of a major difference in sensory patterning between zebrafish and bluefin tuna. Evol. Dev. 14 (2), 204–211.

Gilmour, D.T., Maischein, H.-M., Nüsslein-Volhard, C., 2002. Migration and function of a glial subtype in the vertebrate peripheral nervous system. Neuron 34 (4), 577–588.

Giroux, V., Lento, A.A., Islam, M., Pitarresi, J.R., Kharbanda, A., Hamilton, K.E., et al., 2017. Long-lived keratin 15+ esophageal progenitor cells contribute to homeostasis and regeneration. J. Clin. Invest. 127 (6), 2378–2391.

Giroux, V., Stephan, J., Chatterji, P., Rhoades, B., Wileyto, E.P., Klein-Szanto, A.J., et al., 2018. Mouse intestinal Krt15+ crypt cells are radio-resistant and tumor initiating. Stem Cell Rep. 10 (6), 1947–1958.

Grant, K.A., Raible, D.W., Piotrowski, T., 2005. Regulation of latent sensory hair cell precursors by glia in the zebrafish lateral line. Neuron 45 (1), 69–80.

Haas, P., Gilmour, D., 2006. Chemokine signaling mediates self-organizing tissue migration in the zebrafish lateral line. Dev. Cell 10 (5), 673–680.

Haines, R.L., Lane, E.B., 2012. Keratins and disease at a glance. J. Cell Sci. 125 (Pt 17), 3923–3928.

Hernández, P.P., Moreno, V., Olivari, F.A., Allende, M.L., 2006. Sub-lethal concentrations of waterborne copper are toxic to lateral line neuromasts in zebrafish (Danio rerio). Hear. Res. 213 (1–2), 1–10.

Indjeian, V.B., Kingman, G.A., Jones, F.C., Guenther, C.A., Grimwood, J., Schmutz, J., et al., 2016. Evolving new skeletal traits by cis-regulatory changes in bone morphogenetic proteins. Cell 164 (1–2), 45–56.

Ito, K., Morioka, M., Kimura, S., Tasaki, M., Inohaya, K., Kudo, A., 2014. Differential reparative phenotypes between zebrafish and medaka after cardiac injury. Dev. Dynam. 243 (9), 1106–1115.

Jones, F.C., Grabherr, M.G., Chan, Y.F., Russell, P., Mauceli, E., Johnson, J., et al., 2012. The genomic basis of adaptive evolution in threespine sticklebacks. Nature 484 (7392), 55–61.

Lai, S.L., Marin-Juez, R., Moura, P.L., Kuenne, C., Lai, J.K.H., Tsedeke, A.T., et al., 2017. Reciprocal analyses in zebrafish and medaka reveal that harnessing the immune response promotes cardiac regeneration. Elife 6.

Lancaster, M.A., Renner, M., Martin, C.-A., Wenzel, D., Bicknell, L.S., Hurles, M.E., et al., 2013. Cerebral organoids model human brain development and microcephaly. Nature 501 (7467), 373–379.

Lecaudey, V., Cakan-Akdogan, G., Norton, W.H.J., Gilmour, D., 2008. Dynamic Fgf signaling couples morphogenesis and migration in the zebrafish lateral line primordium. Development 135 (16), 2695–2705.

Ledent, V., 2002. Postembryonic development of the posterior lateral line in zebrafish. Development 129 (3), 597–604.

Liu, Y., Lyle, S., Yang, Z., Cotsarelis, G., 2003. Keratin 15 promoter targets putative epithelial stem cells in the hair follicle bulge. J. Invest. Dermatol. 121 (5), 963–968.

López-Schier, H., Hudspeth, A.J., 2005. Supernumerary neuromasts in the posterior lateral line of zebrafish lacking peripheral glia. Proc. Natl. Acad. Sci. U. S. A 102 (5), 1496–1501.

Lush, M.E., Piotrowski, T., 2014. ErbB expressing Schwann cells control lateral line progenitor cells via non-cell-autonomous regulation of Wnt/β-catenin. eLife 3, e01832.

Lust, K., Wittbrodt, J., 2018. Activating the regenerative potential of Muller glia cells in a regeneration-deficient retina. Elife 7.

Ma, E.Y., Rubel, E.W., Raible, D.W., 2008. Notch signaling regulates the extent of hair cell regeneration in the zebrafish lateral line. J. Neurosci. : Off J. Soc. Neurosci. 28 (9), 2261–2273.

Martinez Arias, A., Steventon, B., 2018. On the nature and function of organizers. Development 145 (5).

McLean, C.Y., Reno, P.L., Pollen, A.A., Bassan, A.I., Capellini, T.D., Guenther, C., et al., 2011. Human-specific loss of regulatory DNA and the evolution of human-specific traits. Nature 471 (7337), 216–219.

Moriyama, Y., Kawanishi, T., Nakamura, R., Tsukahara, T., Sumiyama, K., Suster, M.L., et al., 2012. The medaka zic1/zic4 mutant provides molecular insights into teleost caudal fin evolution. Curr. Biol. 22 (7), 601–607.

Nechiporuk, A., Raible, D.W., 2008. FGF-dependent mechanosensory organ patterning in zebrafish. Science 320 (5884), 1774–1777.

Nogare, D.D., Natesh, N., Chitnis, A., 2019. A Sheath of Motile Cells Supports Collective Migration in of the Zebrafish Posterior Lateral Line Primordium under the Skin, p. 783043 bioRxiv.

Nuñez, V.A., Sarrazin, A.F., Cubedo, N., Allende, M.L., Dambly-Chaudière, C., Ghysen, A., 2009. Postembryonic development of the posterior lateral line in the zebrafish. Evol. Dev. 11 (4), 391–404.

O'Brown, N.M., Summers, B.R., Jones, F.C., Brady, S.D., Kingsley, D.M., 2015. A recurrent regulatory change underlying altered expression and Wnt response of the stickleback armor plates gene EDA. Elife 4, e05290.

Ohtsuka, M., Kikuchi, N., Yokoi, H., Kinoshita, M., Wakamatsu, Y., Ozato, K., et al., 2004. Possible roles of zic1 and zic4, identified within the medaka Double anal fin (Da) locus, in dorsoventral patterning of the trunk-tail region (related to phenotypes of the Da mutant). Mech. Dev. 121 (7–8), 873–882.

Peters, B., Kirfel, J., Bussow, H., Vidal, M., Magin, T.M., 2001. Complete cytolysis and neonatal lethality in keratin 5 knockout mice reveal its fundamental role in skin integrity and in epidermolysis bullosa simplex. Mol. Biol. Cell 12 (6), 1775–1789.

Pichon, F., Ghysen, A., 2004. Evolution of posterior lateral line development in fish and amphibians. Evol. Dev. 6 (3), 187–193.

Pinto-Teixeira, F., Viader-Llargués, O., Torres-Mejía, E., Turan, M., González-Gualda, E., Pola-Morell, L., et al., 2015. Inexhaustible hair-cell regeneration in young and aged zebrafish. Biology open 4 (7), 903–909.

Prud'homme, B., Gompel, N., Rokas, A., Kassner, V.A., Williams, T.M., Yeh, S.D., et al., 2006. Repeated morphological evolution through cis-regulatory changes in a pleiotropic gene. Nature 440 (7087), 1050–1053.

Rembold, M., Loosli, F., Adams, R.J., Wittbrodt, J., 2006. Individual cell migration serves as the driving force for optic vesicle evagination. Science 313 (5790), 1130–1134.

Romero-Carvajal, A., Navajas Acedo, J., Jiang, L., Kozlovskaja-Gumbrienė, A., Alexander, R., Li, H., et al., 2015. Regeneration of sensory hair cells requires localized interactions between the notch and Wnt pathways. Dev. Cell 34 (3), 267–282.

Sánchez, M., Ceci, M.L., Gutiérrez, D., Anguita-Salinas, C., Allende, M.L., 2016. Mechanosensory organ regeneration in zebrafish depends on a population of multipotent progenitor cells kept latent by Schwann cells. BMC Biol. 14 (1), 27.

Sapède, D., Gompel, N., Dambly-Chaudière, C., Ghysen, A., 2002. Cell migration in the postembryonic development of the fish lateral line. Development 129 (3), 605–615.

Sato, T., Vries, R.G., Snippert, H.J., van de Wetering, M., Barker, N., Stange, D.E., et al., 2009. Single Lgr5 stem cells build crypt-villus structures in vitro without a mesenchymal niche. Nature 459 (7244), 262–265.

Seleit, A., Krämer, I., Ambrosio, E., Dross, N., Engel, U., Centanin, L., 2017a. Sequential organogenesis sets two parallel sensory lines in medaka. Development 144 (4), 687–697.

Seleit, A., Krämer, I., Riebesehl, B.F., Ambrosio, E.M., Stolper, J.S., Lischik, C.Q., et al., 2017b. Neural stem cells induce the formation of their physical niche during organogenesis. eLife 6, e29173.

Stemmer, M., Thumberger, T., Del Sol Keyer, M., Wittbrodt, J., Mateo, J.L., 2015. CCTop: an intuitive, flexible and reliable CRISPR/Cas9 target prediction tool. PLoS One 10 (4), e0124633.

Storey, K.G., Crossley, J.M., De Robertis, E.M., Norris, W.E., Stern, C.D., 1992. Neural induction and regionalisation in the chick embryo. Development 114 (3), 729–741.

Sulston, J.E., Schierenberg, E., White, J.G., Thomson, J.N., 1983. The embryonic cell lineage of the nematode Caenorhabditis elegans. Dev. Biol. 100 (1), 64–119.

Sumi, K., Asaoka, R., Nakae, M., Sasaki, K., 2015. Innervation of the lateral line system in the blind cavefish Astyanax mexicanus (Characidae) and comparisons with the eyed surface-dwelling form. Ichthyol. Res. 62 (4), 420–430.

Thermes, V., Grabher, C., Ristoratore, F., Bourrat, F., Choulika, A., Wittbrodt, J., et al., 2002. I-SceI meganuclease mediates highly efficient transgenesis in fish. Mech. Dev. 118 (1–2), 91–98.

Turner, D.A., Baillie-Johnson, P., Martinez Arias, A., 2016. Organoids and the genetically encoded self-assembly of embryonic stem cells. Bioessays : News Rev. Mol, Cell. Dev. Biol. 38 (2), 181–191.

van den Brink, S.C., Baillie-Johnson, P., Balayo, T., Hadjantonakis, A.K., Nowotschin, S., Turner, D.A., et al., 2014. Symmetry breaking, germ layer specification and axial organisation in aggregates of mouse embryonic stem cells. Development 141 (22), 4231–4242.

Wada, H., Ghysen, A., Asakawa, K., Abe, G., Ishitani, T., Kawakami, K., 2013a. Wnt/dkk negative feedback regulates sensory organ size in zebrafish. Curr. Biol. 23 (16), 1559–1565.

Wada, H., Dambly-Chaudière, C., Kawakami, K., Ghysen, A., 2013b. Innervation is required for sense organ development in the lateral line system of adult zebrafish. Proc. Natl. Acad. Sci. Unit. States Am. 110 (14), 5659–5664.

Waddington, C.H., 1941. Evolution of developmental systems. Nature 147 (3717), 108–110.

Waddington, C.H., 1959. Canalization of development and genetic assimilation of acquired characters. Nature 183 (4676), 1654–1655.

Waddington, C.H., 1968. Prolegomena. Towards a Theoretical Biology, : 1. An IUBSSymposium: Biological Sciences & Edinburgh University Press.

Waddington, C.H., 1969. Towards a Theoretical Biology: an IUBS Symposium. Edinburgh University Press, Sketches.

Wark, A.R., Peichel, C.L., 2010. Lateral line diversity among ecologically divergent threespine stickleback populations. J. Exp. Biol. 213 (1), 108–117.

Whitfield, T.T., 2005. Lateral line: precocious phenotypes and planar polarity. Curr. Biol. : CB 15 (2), R67–70.

Wibowo, I., Pinto-Teixeira, F., Satou, C., Higashijima, S-i, López-Schier, H., 2011. Compartmentalized Notch signaling sustains epithelial mirror symmetry. Development 138 (6), 1143–1152.